ning waves" as solutions. The $\Delta_{\vec{k}}$ are slightly inconvenient because the $\Delta_{\vec{k}}$ and $\Delta_{-\vec{k}}$ modes are still coupled in (20). It is possible to make a transformation to "standing wave" modes described by *real* $C_{\vec{k}}$ with the same frequency $\omega_{\vec{k}}$ so that E may be expressed as in (20) but with the $\Delta_{\vec{k}}$ replaced by $C_{\vec{k}}$.[16] The problem is now explicitly reduced to a set of N decoupled harmonic oscillators. We obtain for the magnetization (since $\sum_{i=1}^{N}\theta_i^2=\sum_{\vec{k}'}|\Delta_{k'}|^2=\sum_{\vec{k}'}C_{\vec{k}'}^2$) by (19)

$$\langle m_x\rangle = S\left[1-\frac{1}{2N}\sum_{\vec{k}'}\frac{\int e^{-\beta E}C_{\vec{k}'}^2(\Pi_{BZ}\,dC_{\vec{k}})(\Pi_{BZ}\,dC_{\vec{k}})}{\int e^{-\beta E}(\Pi_{BZ}\,dC_{\vec{k}})(\Pi_{BZ}\,dC_{\vec{k}})}\right]. \tag{21}$$

We are only interested in the low-temperature results, so large amplitudes and velocities should appear with vanishingly small probability. Therefore, we can safely extend the upper limits of the integrals to ∞. With $\Delta_{\vec{k}}$ replaced by $C_{\vec{k}}$ we insert (20) into (21), cancel common factors in the numerator and denominator, evaluate standard integrals, and replace the sum over the BZ by an integral. We are only interested in low temperatures and so only large wavelength (small $|\vec{k}|$) modes should be of importance. Finally, at low temperatures the shape of the BZ should not be important so we can use as an upper limit for our integral k_μ defined by $\pi k_\mu^2=(2\pi/a)^2$ where a is the nearest-neighbor distance. We thus obtain for our two-dimensional systems:

$$\langle m_x\rangle = S\left[1-\frac{1}{\beta}\frac{\rho}{4\pi}\frac{1}{S^2 f_F(0)a^2}\times\ln\left(1+\frac{f_F(0)a^2k_\mu^2}{2(2a_F(0)+B/S)}\right)\right]. \tag{22}$$

Note that if no anisotropies or fields are present $[a_F(0)=B=0]$ then (22) diverges and our spin-wave approximation is inappropriate. This fact was known before Mermin and Wagner proved the magnetization must vanish for this case.

*Research supported in part by the U. S. Atomic Energy Commission, under Contract No. AT(11-1)-427.

†On sabbatical leave (1969–70) from the South Dakota School of Mines and Technology, Rapid City, S. D. 57701.

[1]J. Skalyo, Jr., G. Shirane, R. J. Birgeneau, and H. J. Guggenheim, Phys. Rev. Letters 23, 1394 (1969).

[2]R. J. Birgeneau, H. J. Guggenheim, and G. Shirane, Phys. Rev. Letters 22, 720 (1969).

[3]N. D. Mermin and H. Wagner, Phys. Rev. Letters 17, 1133 (1966).

[4]H. E. Stanley and T. A. Kaplan, Phys. Rev. Letters 17, 913 (1966).

[5]D. Jasnow and M. E. Fisher, Phys. Rev. Letters 23, 286 (1969).

[6]R. E. Watson, M. Blume, and G. H. Vineyard, Phys. Rev. B 2, 684 (1970).

[7]L. Onsager, Phys. Rev. 65, 117 (1944).

[8]M. E. Lines, J. Appl. Phys. 40, 1352 (1969); and references cited therein.

[9]N. D. Mermin, J. Math. Phys. 8, 1061 (1967); see also, M. A. Moore, Phys. Rev. Letters 23, 861 (1969); F. Wegner, Z. Physik 206, 465 (1967); G. Bowers and G. S. Joyce, Phys. Rev. Letters 19, 630 (1967).

[10]D. M. Kaplan and G. C. Summerfeld, Phys. Rev. 187, 639 (1969); and references cited therein; see also, R. E. Watson, M. Blume, and G. H. Vineyard, Phys. Rev. 181, 811 (1969).

[11]V. G. Vaks and A. I. Larkin, Zh. Eksperim. i Teor. Fiz. 49, 975 (1965) [Sov. Phys. JETP 22, 678 (1966)].

[12]P. C. Hohenberg, Phys. Rev. 158, 383 (1967).

[13]H. Wagner, Z. Physik 195, 273 (1966).

[14]N. D. Mermin, Phys. Rev. 176, 250 (1968); N. D. Mermin, Ref. 9.

[15]C. Kittel, *Quantum Theory of Solids* (Wiley, New York, 1963), Chap. 4.

[16]C. Kittel, Ref. 16, Chap. 1.

PHYSICAL REVIEW B VOLUME 3, NUMBER 9 1 MAY 1971

Paramagnetic and Antiferromagnetic Phases in the Half-Filled Narrow Energy Band*

Laurent G. Caron† and G. Kemeny‡
Department of Electrical Engineering, Massachusetts Institute of Technology, Cambridge, Massachusetts 02139
(Received 8 October 1969)

The effect of correlation on the antiferromagnetic and paramagnetic phases of Hubbard's model of a half-filled narrow band are investigated using second-order perturbation theory. Employing the gap of the antiferromagnetic state as a variational parameter, it is shown that the increase of the bandwidth/potential-energy ratio leads to a phase transition into the paramagnetic state nearly where Mott has estimated it to occur. The convergence of the perturbation expansion is shown to be excellent at the transition.

I. INTRODUCTION

In a recent paper[1] the authors discussed the mathematical methods they believed necessary for the treatment of the paramagnetic and antiferromagnetic ranges of the Hubbard Hamiltonian[2] in a half-filled narrow band. They argued that a t-matrix expansion would be required in the investi-

gation of the short-range correlation effects. A cursory examination of our results seemed to bear out our guess that a reaction-matrix expansion would converge faster than a bare interaction one. For the special case which we computed, i.e., a simple cubic lattice in the tight-binding limit, a closer scrutiny revealed that quite the opposite was true at the paramagnet-antiferromagnet transition. This obliged us to revert to ordinary second-order perturbation theory.

In this paper we treat two possible physical states of the half-filled narrow energy band using the Hubbard Hamiltonian,[2]

$$H=\sum_{ij}\sum_{\sigma}T_{ij}C_{i\sigma}^{\dagger}C_{j\sigma}+I\sum_{i}n_{i+}n_{i-}. \tag{1.1}$$

These are the paramagnetic and antiferromagnetic states. The ground state of the system is decided by the minimization of the total energy with the antiferromagnetic gap as a variational parameter. When the gap so determined is zero, the paramagnetic state is stable. We first examine the Hubbard Hamiltonian on a simple cubic lattice within the Hartree approximation. We then consider the effects of short-range electron correlation using a second-order perturbation calculation restricted to the tight-binding limit. There follows a discussion of the convergence of the expansion and a comparative analysis of the t-matrix approximation.

All calculations are at the absolute zero of temperature. We shall use the Goldstone diagram technique as reviewed in Day's[3] paper.[4,5] We have also normalized the interatomic distance to 1.

II. HARTREE APPROXIMATION

As a first approximation, one may be tempted to neglect the effects of correlation. This is the Hartree approximation in which each particle is in a stationary eigenstate. This sets a variational upper bound to the system's energy.

Following Day[3] we add and subtract a single-particle potential $V_{ij\sigma}$ to the Hamiltonian equation (1.1),

$$H=H_0+H_1, \tag{2.1}$$

$$H_0=\sum_{ij}\sum_{\sigma}(T_{ij}+V_{ij\sigma})C_{i\sigma}^{\dagger}C_{j\sigma}, \tag{2.2}$$

$$H_1=I\sum_{i}n_{i+}n_{i-}-\sum_{ij}\sum_{\sigma}V_{ij\sigma}C_{i\sigma}^{\dagger}C_{j\sigma}. \tag{2.3}$$

One chooses this potential to achieve magnetic polarization on the band and/or faster convergence of the perturbation expansion of the energy. Wishing to examine the antiferromagnetically polarized state of a simple cubic lattice we set

$$V_{ij\pm}=\pm\tfrac{1}{2}\Delta\, e^{i\vec{\pi}\cdot\vec{R}_i}\delta_{ij}, \tag{2.4}$$

where

$$\vec{\pi}=\pi(\hat{X}+\hat{Y}+\hat{Z}). \tag{2.5}$$

The unperturbed Hamiltonian H_0 is then diagonalized by the following canonical transformation:

$$C_{i\pm}=\sum_{\vec{k}}\Phi_{\vec{k}\pm}(\vec{R}_i)a_{\vec{k}\pm}$$

$$=N^{-1/2}\sum_{\vec{k}}e^{i\vec{k}\cdot\vec{R}_i}(A_{\vec{k}}\mp B_{\vec{k}}e^{i\vec{\pi}\cdot\vec{R}_i})a_{\vec{k}\pm}, \tag{2.6}$$

where

$$A_{\vec{k}}=\sqrt{\tfrac{1}{2}}\left(1-\frac{S_{\vec{k}}(\epsilon_{\vec{k}}-\epsilon_{\vec{k}+\vec{\pi}})}{[\Delta^2+(\epsilon_{\vec{k}}-\epsilon_{\vec{k}+\vec{\pi}})^2]^{1/2}}\right)^{1/2}, \tag{2.7}$$

$$B_{\vec{k}}=\sqrt{\tfrac{1}{2}}\,S_{\vec{k}}\left(1+\frac{S_{\vec{k}}(\epsilon_{\vec{k}}-\epsilon_{\vec{k}+\vec{\pi}})}{[\Delta^2+(\epsilon_{\vec{k}}-\epsilon_{\vec{k}+\vec{\pi}})^2]^{1/2}}\right)^{1/2}, \tag{2.8}$$

$$S_{\vec{k}}=\frac{\cos k_X+\cos k_Y+\cos k_Z}{|\cos k_X+\cos k_Y+\cos k_Z|}, \tag{2.9}$$

$$\epsilon_{\vec{k}}=\sum_{j}T_{ij}e^{i\vec{k}\cdot(\vec{R}_j-\vec{R}_i)}. \tag{2.10}$$

The summation over $\vec{k}$ extends throughout the first Brillouin zone. The eigenvalues are

$$E_{\vec{k}}=\tfrac{1}{2}\{(\epsilon_{\vec{k}}+\epsilon_{\vec{k}+\vec{\pi}})-S_{\vec{k}}[\Delta^2+(\epsilon_{\vec{k}}-\epsilon_{\vec{k}+\vec{\pi}})^2]^{1/2}\}. \tag{2.11}$$

The next step towards the Hartree approximation is to add to the zero-order energy those terms corresponding to the first-order Goldstone diagrams of Fig. 1.[4] The diagram rules for an S band are summarized in Appendix A. The end result is

$$E_H=\sum_{\sigma}\sum_{\vec{k}<\vec{k}_F}E_{\vec{k}}+I\sum_{\vec{k}_1;\vec{k}_2<\vec{k}_F}\sum_{i}\Phi_{\vec{k}_1+}^{*}(\vec{R}_i)\Phi_{\vec{k}_2-}^{*}(\vec{R}_i)$$
$$\times\Phi_{\vec{k}_2-}(\vec{R}_i)\Phi_{\vec{k}_1+}(\vec{R}_i)$$
$$-\tfrac{1}{2}\Delta\sum_{\vec{k}_1<\vec{k}_F}\sum_{i}\Phi_{\vec{k}_1+}^{*}(\vec{R}_i)\Phi_{\vec{k}_1+}(\vec{R}_i)e^{i\vec{\pi}\cdot\vec{R}_i}$$
$$+\tfrac{1}{2}\Delta\sum_{\vec{k}_2<\vec{k}_F}\sum_{i}\Phi_{\vec{k}_2-}^{*}(\vec{R}_i)\Phi_{\vec{k}_2-}(\vec{R}_i)e^{i\vec{\pi}\cdot\vec{R}_i}, \tag{2.12}$$

where $\vec{k}_F$ is on the Fermi surface. The requirement that E_H be an extremum with respect to the variational parameter Δ yields the Matsubara self-consistency relation[6]

$$\Delta=2IN^{-1}\Delta\sum_{\vec{k}<\vec{k}_F}\frac{S_{\vec{k}}}{[\Delta^2+(\epsilon_{\vec{k}}-\epsilon_{\vec{k}+\vec{\pi}})^2]^{1/2}}. \tag{2.13}$$

This self-consistency condition has two solutions. The trivial one $\Delta=0$ is for the paramagnetic state. A lower-energy one, when it exists, for $\Delta\neq 0$ corresponds to the antiferromagnetic state.

In order to get an idea about the stability of the antiferromagnetic state we have focused our at-

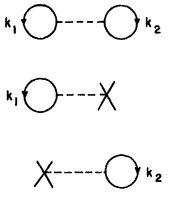

FIG. 1. First-order Goldstone diagrams.

tention on the critical hopping strength at the onset of antiferromagnetism. At the transition, the energy gap Δ is zero and the self-consistency condition is reduced to

$$2IN^{-1}\sum_{\vec{k}<\vec{k}_F}\frac{S_{\vec{k}}}{|\epsilon_{\vec{k}}-\epsilon_{\vec{k}+\vec{\pi}}|}=1. \tag{2.14}$$

We have computed a special case with first- and second-nearest-neighbor hopping only. Dropping the constant energy contribution of T_{ii} the band energy becomes

$$E_{\vec{k}}=-2T_1(\cos k_x+\cos k_y+\cos k_z)$$
$$-4T_2(\cos k_x\cos k_y+\cos k_x\cos k_y+\cos k_y\cos k_z). \tag{2.15}$$

The resulting phase diagram is shown in Fig. 2. We have used the dimensionless parameter

$$C=4T_1/I \tag{2.16}$$

as a measure of hopping strength.

There emerges the conclusion that antiferromagnetism is favorable at narrow bandwidths. The Hubbard Hamiltonian is then consistent with the observed antiferromagnetism of narrow bands such as in the transition-metal oxides.[7] However at smaller second-to-first-nearest-neighbor hopping ratios that would be expected of narrow bands, the critical hopping strength for onset of paramagnetism seems preposterously large. It even goes to infinity as T_2/T_1 goes to zero, implying that the tight-binding limit of Hubbard's Hamiltonian would be exclusively antiferromagnetic at zero temperature for the half-filled band.[6,8,9] Of course this would have little experimental implication, since the limit of large bandwidths is only a philosophical extension of a model, incomplete at that, of a narrow-band crystal. But this same model when viewed as a theoretical entity does warrant a thorough investigation. One has to consider the effect of short-range correlation on the energy in order to determine conclusively the behavior of the band.

We then propose to study the tight-binding limit

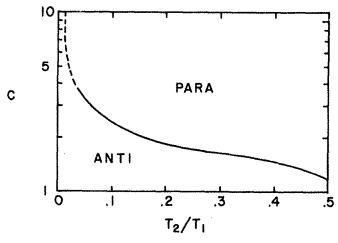

FIG. 2. Antiferromagnetic-paramagnetic phase diagram in the Hartree approximation. Hopping strength $C=4T_1/I$ as a function of second-to-first-nearest-neighbor hopping ratio.

of the Hubbard model including short-range correlation effects to second order in the interaction. This should settle the uneasiness about the long-range magnetic behavior of the model.

III. SECOND-ORDER PERTURBATION THEORY

Restricting the second-order perturbation calculation to only nearest-neighbor hopping has the advantage of simplifying the zero-order states. The eigenstates and eigenvalues are

$$\Phi_{\vec{k}\pm}(\vec{R})=N^{-1/2}e^{i\vec{k}\cdot\vec{R}}(A_{\vec{k}}\mp B_{\vec{k}}e^{i\vec{\pi}\cdot\vec{R}}), \tag{3.1}$$

$$E_{\vec{k}}=-\tfrac{1}{2}S_{\vec{k}}(\Delta^2+4\epsilon_{\vec{k}}^2)^{1/2}, \tag{3.2}$$

$$A_{\vec{k}}=\sqrt{\tfrac{1}{2}}\left(1-\frac{2S_{\vec{k}}\epsilon_{\vec{k}}}{[\Delta^2+4\epsilon_{\vec{k}}^2]^{1/2}}\right)^{1/2}, \tag{3.3}$$

$$B_{\vec{k}}=S_{\vec{k}}\left(1+\frac{2S_{\vec{k}}\epsilon_{\vec{k}}}{[\Delta^2+4\epsilon_{\vec{k}}^2]^{1/2}}\right)^{1/2}, \tag{3.4}$$

$$\epsilon_{\vec{k}}=-2T(\cos k_x+\cos k_y+\cos k_z), \tag{3.5}$$

$$S_{\vec{k}}=-\epsilon_{\vec{k}}/|\epsilon_{\vec{k}}|. \tag{3.6}$$

For the half-filled band, the Fermi surface is defined by

$$\epsilon_{\vec{k}}=0, \tag{3.7}$$

and the energy gap at this surface is Δ.

The Goldstone diagram contributing the correlation effects to second-order in the interaction is shown in Fig. 3.[5] Following the diagrammatic rules,

$$E_2=E_H-I^2\sum_{\vec{k}_1\vec{k}_2<\vec{k}_F}\sum_{\vec{k}_1'\vec{k}_2'<\vec{k}_F}\sum_i\Phi^*_{\vec{k}_1'+}(\vec{R}_i)\Phi^*_{\vec{k}_2'-}(\vec{R}_i)$$
$$\times\frac{\Phi_{\vec{k}_2-}(\vec{R}_i)\Phi_{\vec{k}_1+}(\vec{R}_i)}{E_{\vec{k}_1'}+E_{\vec{k}_2'}-E_{\vec{k}_1}-E_{\vec{k}_2}}. \tag{3.8}$$

This energy is minimized with respect to the variational parameter Δ. The results are summarized in Figs. 4–6. We are again using the dimensionless parameter $C=4T/I$ as a measure of bandwidth. One observes a transition from an antiferromagnet ($\Delta\neq0$) to a paramagnetic ($\Delta=0$) at

$$C_{CR}=1.1\pm0.2. \tag{3.9}$$

This transition is apparently of first-order because of the collapse in the energy gap. The uncertainty in the critical value is due to a numerical inaccuracy in energy of

$$\Delta(E/NT)\simeq\pm0.005/C^2. \tag{3.10}$$

This also plays a role on the determination of the order of the transition. Because of the small energy difference involved near the transition the energy minimum, thus the gap, cannot be determined conclusively. As the energy uncertainty is of the order of the thermal energy the question really becomes academic since one would indeed

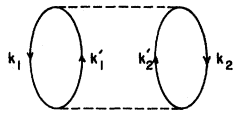

FIG. 3. Goldstone diagram representing short-range correlation effects to second order.

have to go to absolute zero to determine the order of the transition experimentally.

There are three effects of electron correlation to second-order perturbation theory: (a) There is an appreciable energy lowering. This was expected since the Hartree approximation only sets an upper bound to the energy. (b) There is a large decrease of the energy gap in the antiferromagnetic state. It is apparently worthwhile to exchange some long-range order for some short-range order. (c) There is also the occurrence of an antiferromagnetic-paramagnetic phase transition contrary to expectations based on the Hartree approximation. In fact the critical bandwidth/potential-energy ratio is smaller than even the most optimistic Hartree prediction for large second-nearest-neighbor hopping strength.

It might be informative to compare our transition with the estimate of Mott.[10] He argued that in a hydrogen lattice the transition occurs at an interatomic distance of

$$R \simeq 4.5 \text{ bohr}. \tag{3.11}$$

On the basis of Slater's[11] solution of the hydrogen $1S$ integrals, we can evaluate the intra-atomic interaction strength at

$$I \simeq 1.25 \text{ Ry} \tag{3.12}$$

and the hopping integral, as a function of inter-

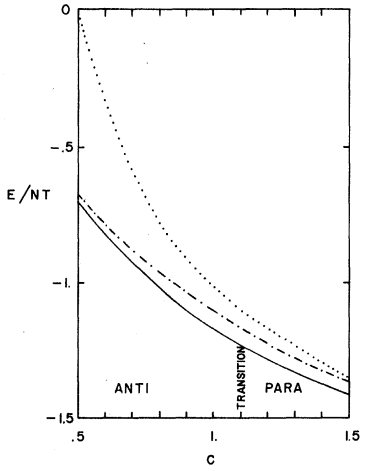

FIG. 4. Energy per electron in units of T in the paramagnetic Hartree (dotted line), antiferromagnetic Matsubara (dot-dashed line), and variational second-order approximations (solid line). The bandwidth/potential-energy ratio is $3C$.

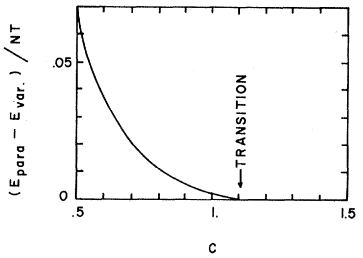

FIG. 5. Energy difference per electron in units of T between the paramagnetic and variational states to second order. The bandwidth/potential-energy ratio is $3C$.

atomic distance R, as

$$T = -\int d\vec{r}\, a(\vec{r})(-\nabla^2 - 2/r_{1a} - 2/r_{1b})b(\vec{r})$$
$$= e^{-R}(3 + 3R + \tfrac{1}{3}R^2) \text{ Ry}, \tag{3.13}$$

where $a(\vec{r})$, $b(\vec{r})$ are $1S$ hydrogen orbitals centered on nearest-neighbor atoms. Our estimate of the interatomic distance at the transition is then

$$R = 4.1 \pm 0.2 \text{ bohr}, \tag{3.14}$$

which is close to the estimate of Mott.

One must now investigate the reliability of the second-order energy correction in order to assess the credibility of the above conclusions.

IV. CONVERGENCE OF PERTURBATION EXPANSION

The criterion for the convergence of the bare-interaction perturbation expansion is that adopted by Day.[3] On addition of an interaction line to an existing diagram one gets a higher-order diagram. If the energy contribution of this new diagram is much smaller than that of the original one, then convergence is to be expected.

It is possible to estimate the energy ratio of the new to the old diagrams. Consider a typical diagram as in Fig. 7 where the hatched areas represent the lower and upper parts of the original dia-

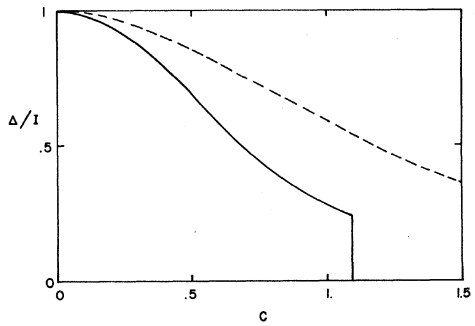

FIG. 6. Energy gap in units of the interaction strength for the antiferromagnetic Matsubara (dashed line) and variational second-order approximations (solid line). The bandwidth/potential-energy ratio is $3C$.

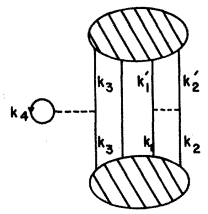

FIG. 7. Diagram used to calculate the effect of inserting an additional interaction to an existing diagram.

gram, linked by the $\vec{k}_1, \vec{k}_2, \vec{k}_3$ particle lines. One can typically add a bare interaction between two existing particle lines or a bubble interaction to a particle line. In the first case one encounters an additional factor of absolute value

$$\xi_1 = I \sum_{\vec{k}_1' \vec{k}_2'} \sum_i \Phi^*_{\vec{k}_1'\sigma}(\vec{R}_i)\Phi^*_{\vec{k}_2'-\sigma}(\vec{R}_i)\Phi_{\vec{k}_2-\sigma}(\vec{R}_i)\Phi_{\vec{k}_1\sigma}(\vec{R}_i)/e \tag{4.1}$$

and in the second,

$$\xi_2 = I \sum_i \sum_{\vec{k}_4 < k_F} \Phi^*_{\vec{k}_3\sigma}(\vec{R}_i)\Phi^*_{\vec{k}_4-\sigma}(\vec{R}_i)\Phi_{\vec{k}_4-\sigma}(\vec{R}_i)\Phi_{\vec{k}_3\sigma}(\vec{R}_i)/e\,. \tag{4.2}$$

Therefore

$$\xi = \frac{\text{contribution of higher-order diagram}}{\text{contribution of original diagram}} \tag{4.3}$$

$$\approx \begin{cases} \xi_1 & \text{interaction between existing particle lines} \\ \xi_2 & \text{bubble interaction.} \end{cases} \tag{4.4}$$

A. Paramagnetic State

These factors can be approximated in the paramagnetic half-filled band by taking an average value,

$$\xi_1 \approx I \langle 1/e \rangle N^{-1} \sum_{\vec{k}_1' \vec{k}_2'} \sum_{\vec{G}} \delta(\vec{k}_1 + \vec{k}_2 - \vec{k}_1' - \vec{k}_2' + \vec{G}) \approx \tfrac{1}{2} I \langle 1/e \rangle\,, \tag{4.5}$$

$$\xi_2 \approx \tfrac{1}{2} I \langle 1/e \rangle \approx \xi_1\,, \tag{4.6}$$

where $\vec{G}$ is a reciprocal-lattice vector. The factors of $\frac{1}{2}$ originate from the restriction of any particle type to half the Brillouin zone. As each energy denominator e contains at least four contributions, we estimate that

$$\langle 1/e \rangle \lesssim 1/8T; \tag{4.7}$$

therefore

$$\xi \lesssim 1/4C\,. \tag{4.8}$$

One can then expect convergence for $C \gtrsim 1$ on the basis of this rough estimate alone.

As mentioned in the Introduction, the possibility of a faster converging reaction-matrix expansion must be considered. Interpreting the additional interactions in Fig. 7 as a reaction matrix G and referring to Appendix B, it can be deduced that

$$\xi \approx N^{-1} \sum_{\vec{k}_1' \vec{k}_2'} \sum_{\vec{G}} \delta(\vec{k}_1 + \vec{k}_2 - \vec{k}_1' - \vec{k}_2' + \vec{G}) \left\langle \vec{k}_1' \vec{k}_2' \left| \frac{G}{e} \right| \vec{k}_1 \vec{k}_2 \right\rangle. \tag{4.9}$$

However since

$$(G/e)\,|\vec{k}_1 \vec{k}_2\rangle = (I/e)\,|\psi_{\vec{k}_1 \vec{k}_2}\rangle\,, \tag{4.10}$$

we find

$$\xi = I \sum_i \Phi^*_{\vec{k}_1'\sigma}(\vec{R}_i)\Phi^*_{\vec{k}_2'-\sigma}(\vec{R}_i)\Psi_{\vec{k}_1\vec{k}_2}(\vec{R}_i\vec{R}_i)/e\,, \tag{4.11}$$

where $\psi_{\vec{k}_1\vec{k}_2}(\vec{R}_1\vec{R}_2)$ and $\Phi_{\vec{k}_1\sigma}(\vec{R}_1)\Phi_{\vec{k}_2-\sigma}(\vec{R}_2)$ are the reaction-matrix-corrected and unperturbed pair wave functions, respectively. Averaging,

$$\xi \lesssim \langle \textstyle\sum_i \Phi^*_{\vec{k}_1'\sigma}(\vec{R}_i)\Phi^*_{\vec{k}_2'-\sigma}(\vec{R}_i)\psi_{\vec{k}_1\vec{k}_2}(\vec{R}_i\vec{R}_i) \rangle / 4C\,. \tag{4.12}$$

Since the pair wave function on the same site is reduced by correlation effects it follows the reaction-matrix convergence ratio ξ is smaller than the one given by second-order perturbation theory.

For comparison purposes we have plotted the convergence parameters in Fig. 8. The pair wave function used in Eq. (4.12) was calculated on the energy shell as in Eq. (B8). We have adjusted the proportionality constant implicit in Eqs. (4.8) and (4.12) so that the value of ξ for the reaction-matrix expansion in the limit $I \to \infty$ agrees with Day's estimate of 1. Our own estimate seems to overemphasize the size of the convergence ratio. It would appear a reaction-matrix expansion converges faster than a bare-interaction one. Whereas the reaction matrix would converge for $C \gtrsim 0.4$, the bare interaction would do so only for $C \gtrsim 0.6$. We have taken as a rule of thumb that convergence occurs for $\xi \lesssim 0.3$. This is consistent with the occurrence of bound electron-hole pairs for $C \lesssim 0.3$.[2,12] In this range convergence is not expected. The preceding conclusion is misleading as it would lead one to believe that a reaction-matrix expansion is preferable. It turns out that the special problem we have treated lends itself to a treatment based on the theorem of Appendix C. All odd orders in the bare-interaction perturbation expansion are absent. One would then have to go to fourth order to find the next energy correction

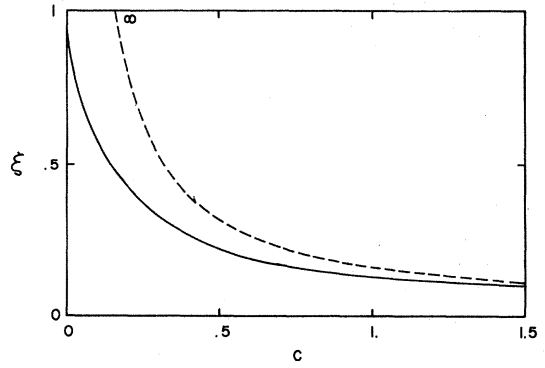

FIG. 8. Convergence parameter for the bare interaction (dashed line) and reaction-matrix expansions (solid line).

to the paramagnetic state. It would be smaller by a factor ξ^2 than the second-order correction. At the phase transition, one would expect the energy correction to be

$$\xi^2 (E_2 - E_H)/NT \approx 0.003, \tag{4.13}$$

which is outside the reach of our numerical accuracy and also much less than the energy differences involved near the transition. This would give the bare-interaction expansion an edge over the reaction-matrix one, at least in the paramagnetic state.

B. Antiferromagnetic State

The convergence parameter ξ as defined in Eqs. (4.1) and (4.2) is sensitive to the nature of the particles involved, i.e., electrons or holes, in the antiferromagnetic phase. At worst one can estimate that for the half-filled band

$$\xi \lesssim \tfrac{1}{2} I \langle 1/e \rangle \lesssim \tfrac{1}{2}. \tag{4.14}$$

It is the energy gap at the Fermi surface which has this drastic effect of setting a lower bound to the energy denominator. On the average the energy difference between an electron in the upper half of the antiferromagnetically split band and a hole in the lower half is of the order of I. Long-range order is so natural to the system that a bare-interaction expansion is convergent on our variational antiferromagnetic state. This convergence parameter eventually merges with the paramagnetic one for a small enough gap.

The theorem invoked for the disappearance of odd-order contributions to the paramagnetic energy cannot be called upon here. But it can be argued that close to the transition, when the gap Δ is smaller, near cancellation of odd-order terms is probable. It is estimated the energy correction from left-over diagrams to third order would be smaller than our numerical uncertainty.

C. Conclusion

The conclusion to be drawn from the convergence analysis is that a second-order approximation is excellent in the tight-binding limit for $C \gtrsim 0.5$ and is probably very good for small values of second-nearest-neighbor hopping.

V. DISCUSSION

The Hartree approximation yielded the basic information as to the antiferromagnetic ground-state tendencies of the Hubbard Hamiltonian. However its forecast of the onset of the antiferromagnetic phase is off by a large amount especially near the tight-binding limit of the Hamiltonian. This stresses the importance of short-range correlation effects in systems with strong short-range forces.

One may now ponder the special conditions operating in this treatment of the half-filled Hubbard band. The symmetry of the unperturbed tight-binding band energies leads to the disappearance of odd-order perturbation terms. This favors a convergent ordinary perturbation expansion over a reaction-matrix one. From the discussion in Appendix B, it turns out that even under these special conditions the t-matrix approximation would have been almost as good. Under normal conditions the latter approximation would, in fact, be preferable as it would converge faster and also at smaller bandwidth. It must also be considered that, this being a high-density system, an expansion on the paramagnetic state is divergent for large enough interaction strength. It was then a happy outcome that the paramagnetic state became unstable in favor of an antiferromagnetic state before the interaction could have drastic effects on convergence. Had it not been so we could still have concluded the occurrence of a transition but its exact whereabouts would have been unknown. Now what of a partially filled band? For smaller electron or hole occupancies, the t-matrix approximation would be indicated as it is the first term in an expansion in the density. It would then seem that this approximation should be preferred for a phase study of the Hubbard Hamiltonian as a function of occupancy.

ACKNOWLEDGMENTS

The authors are indebted to Professor G. W. Pratt, Jr., for the hospitality extended to them at the Massachusetts Institute of Technology. One of the authors (L. G. C.) wishes to thank Laura Roth for a helpful discussion. The initial stages of this work were performed at Ledgemont Laboratory, Kennecott Copper Corp., Lexington, Mass. The numerical calculations were performed at the University of Sherbrooke Computation Center.

APPENDIX A: GOLDSTONE DIAGRAM RULES FOR HUBBARD HAMILTONIAN

The following rules are a version of those presented by Day.[3] They have been adapted to Hubbard's Hamiltonian [Eqs. (2.1)–(2.11)].

(a) An upward directed line represents an occupied state (electron) above the Fermi sea. A downward directed line represents an unoccupied state (hole) in the Fermi sea.

(b) With every horizontal dashed interaction line between opposite-spin particles there is an associated factor

$$I \sum_i \Phi^*_{\vec{k}_1'\sigma}(\vec{R}_i)\, \Phi^*_{\vec{k}_2'-\sigma}(\vec{R}_i)\, \Phi_{\vec{k}_2-\sigma}(\vec{R}_i)\, \Phi_{\vec{k}_1\sigma}(\vec{R}_i), \tag{A1}$$

where $\Phi_{\vec{k}\sigma}(\vec{R})$ is a zero-order eigenfunction. $\vec{k}_1$, $\vec{k}_2$ and $\vec{k}_1'$, $\vec{k}_2'$ are the incoming and scattered particle momenta, respectively.

(c) With every interaction line between a particle

of spin σ and the one-body potential, there is an associated factor

$$\sum_{ij} \Phi^*_{\vec{k}'\sigma}(\vec{R}_i) V_{ij\sigma} \Phi_{\vec{k}\sigma}(\vec{R}_j). \tag{A2}$$

$\vec{k}$ and $\vec{k}'$ are the incoming and outgoing momenta, respectively.

(d) The energy denominator e associated with every one but the last interaction is equal to the sum of the electron energies minus the hole energies.

(e) The sign of the contribution of any diagram is given by

$$(-1)^{h+l+e+u}, \tag{A3}$$

where h is the number of hole lines, l is the number of closed loops, e is the number of energy denominators, and n is the number of one-body interactions.

APPENDIX B: REACTION MATRIX

The essence of the reaction-matrix expansion is to replace the bare interaction by an effective G interaction in which all possible electron pair scattering above the Fermi sea is taken into account. This G matrix is defined as

$$G = v - v(Q/e)v + v(Q/e)v(Q/e)v \ldots, \tag{B1}$$

where v is the bare interaction in the momentum representation. The Q operator limits the scattered particles above the Fermi surface.

Following Day[3] we define the state vector for two such particles in momentum space,

$$|\psi_{\vec{k}_1\vec{k}_2}\rangle = |\Phi_{\vec{k}_1}\Phi_{\vec{k}_2}\rangle - (Q/e)G\,|\Phi_{\vec{k}_1}\Phi_{\vec{k}_2}\rangle, \tag{B2}$$

from which

$$v\,|\psi_{\vec{k}_1\vec{k}_2}\rangle = G\,|\Phi_{\vec{k}_1}\Phi_{\vec{k}_2}\rangle. \tag{B3}$$

Therefore

$$|\psi_{\vec{k}_1\vec{k}_2}\rangle = |\Phi_{\vec{k}_1}\Phi_{\vec{k}_2}\rangle - (Q/e)v\,|\psi_{\vec{k}_1\vec{k}_2}\rangle. \tag{B4}$$

In the reaction-matrix expansion, diagram rule (b) is then modified accordingly: With every horizontal G-matrix interaction between opposite-spin particles there is an associated factor

$$\langle \Phi_{\vec{k}_1'}\Phi_{\vec{k}_2'}|\, G\,|\,\Phi_{\vec{k}_1}\Phi_{\vec{k}_2}\rangle. \tag{B5}$$

In the t-matrix approximation one is interested in the first-order term of the G-matrix expansion. The Goldstone diagram series in the bare interaction representing this approximation is shown in Fig. 9.[5] For such a calculation on the energy shell,

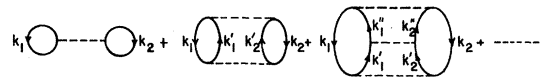

FIG. 9. Goldstone diagrams contributing to the t-matrix approximation.

the energy is

$$E_t = \sum_\sigma \sum_{\vec{k}<\vec{k}_F} E_{\vec{k}} + \sum_{\vec{k}_1\vec{k}_2<\vec{k}_F} \langle \Phi_{\vec{k}_1}\Phi_{\vec{k}_2}\,|\,G\,|\,\Phi_{\vec{k}_1}\Phi_{\vec{k}_2}\rangle$$
$$= \sum_\sigma \sum_{\vec{k}<\vec{k}_F} E_{\vec{k}} + \sum_{\vec{k}_1\vec{k}_2<\vec{k}_F} \langle \Phi_{\vec{k}_1}\Phi_{\vec{k}_2}\,|\,v\,|\,\Psi_{\vec{k}_1\vec{k}_2}\rangle. \tag{B6}$$

For the case of the Hubbard Hamiltonian this expression in configuration space becomes

$$E_t = \sum_\sigma \sum_{\vec{k}<\vec{k}_F} E_{\vec{k}} + I \sum_{\vec{k}_1\vec{k}_2<\vec{k}_F} \sum_i \Phi^*_{\vec{k}_1+}(\vec{R}_i)\,\Phi^*_{\vec{k}_2-}(\vec{R}_i) \times \Psi_{\vec{k}_1\vec{k}_2}(\vec{R}_i\vec{R}_i), \tag{B7}$$

where, from Eq. (B4),

$$\psi_{\vec{k}_1\vec{k}_2}(\vec{R}_1\vec{R}_2) = \Phi_{\vec{k}_1+}(\vec{R}_1)\,\Phi_{\vec{k}_2-}(\vec{R}_2) - I \sum_{\vec{k}_1'\vec{k}_2'<\vec{k}_F} \Phi_{\vec{k}_1'+}(\vec{R}_1)\Phi_{\vec{k}_2'-}(\vec{R}_2) \times \sum_i \frac{\Phi^*_{\vec{k}_1'+}(\vec{R}_i)\,\Phi^*_{\vec{k}_2'-}(\vec{R}_i)\,\psi_{\vec{k}_1\vec{k}_2}(\vec{R}_i\vec{R}_i)}{E_{\vec{k}_1'} + E_{\vec{k}_2'} - E_{\vec{k}_1} - E_{\vec{k}_2}}. \tag{B8}$$

For the sake of completeness we have computed the t-matrix energy for the paramagnetic state, in the tight-binding limit. In Fig. 10 we compare the results to the variational second-order calculation of Sec. III. The t-matrix energy is seen to be larger although it rapidly converges to the second-order value near $C = 1$. The energy difference, though small, would be sufficient to shift the phase transition to a larger value of the bandwidth,

$$C_{CR} = 1.4 \pm 0.2. \tag{B9}$$

Although this does not appear too significant a difference it is nevertheless soothing to know the second-order approximation is ever so slightly better.

APPENDIX C: SPECIAL THEOREM

The following theorem and corollary on the Goldstone diagrams apply to a translationally invariant state of the simple cubic lattice in the tight-binding limit.

Theorem. Under the above restrictions, all Goldstone diagrams[5] containing at least one closed loop with an odd number ($\neq 1$) of particle lines vanish.

Proof. Consider such a loop consisting of n electron and m hole lines and $n+m$ = odd vertices.

(a) For a translationally invariant system, at each vertex one has an associated momentum-conserving condition involving at least two lines $\vec{k}_1$ and $\vec{k}_1'$ of the loop

$$\sum_{\vec{G}} \delta(\vec{k}_a' + \vec{k}_1' - \vec{k}_1 - \vec{k}_a + \vec{G}), \tag{C1}$$

where $\vec{G}$ is any reciprocal-lattice vector.

(b) There is an associated energy denominator

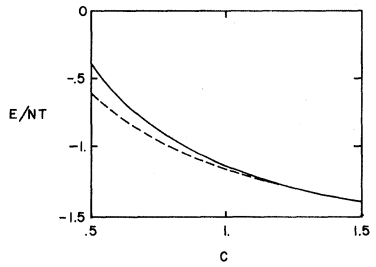

FIG. 10. Energy per electron in units of T for the paramagnetic second-order (dashed line) and paramagnetic t-matrix approximations (solid line). The bandwidth/potential-energy ratio is $3C$.

involving the energies of at least two particles $\vec{k}_1'$ and $\vec{k}_2$ of the loop

$$e = (\pm \epsilon_{\vec{k}_1'} \pm \epsilon_{\vec{k}_2} + \text{other terms}) . \tag{C2}$$

The upper sign is for an electron line and the lower for a hole line.

(c) There is also a $(-1)^m$ sign accompanying the m hole lines of the loop.

The tight-binding energy, Eq. (3.5), is such that the Fermi surface of a half-filled band is given by

$$\epsilon_{\vec{k}_F} = 0 . \tag{C3}$$

Moreover, we have

$$\epsilon_{\vec{k}} = -\epsilon_{\vec{k}+\vec{\pi}} . \tag{C4}$$

Thus if $\vec{k}$ is an electron momentum, then $\vec{k}+\vec{\pi}$ is a hole momentum. Here $\vec{\pi}$ is any of the eight vectors

$$\vec{\pi} = \pi(\pm\hat{x} \pm \hat{y} \pm \hat{z}) \tag{C5}$$

such that $\vec{k}+\vec{\pi}$ is within the first Brillouin zone. The reciprocal is also true.

Let us now invert the direction of the lines in the loop, i.e., change holes into electrons and vice versa, by replacing every $\vec{k}$ by a $\vec{k}+\vec{\pi}$. One gets a topologically different diagram since there are now m electron and n hole lines. The bubble-interaction loop $n+m=1$ is the only exception since such an inversion is illegal.

(i) At each vertex, the momentum-conserving condition becomes

$$\sum_{\vec{G}} \delta(\vec{k}_a' + (\vec{k}_1' + \vec{\pi}) - (\vec{k}_1 + \vec{\pi}) - \vec{k}_a + \vec{G}) . \tag{C6}$$

The extra factors of $\vec{\pi}$ get absorbed in the summation over $\vec{G}$ and thus, independently of $\vec{k}_a$ and $\vec{k}_a'$; this condition is the same as (C1).

(ii) The associated energy denominator is

$$e = (\mp \epsilon_{\vec{k}_1+\vec{\pi}} \mp \epsilon_{\vec{k}_2+\vec{\pi}} + \text{other terms}). \tag{C7}$$

The sign coefficients of the energies have been inverted since the nature of the particle lines has changed. Because of the symmetry of the hopping energy, Eq. (C4), this energy denominator is identical to the previous one (C2), independently of the other terms.

(iii) There is now a $(-1)^n$ sign accompanying the n hole lines of the new loop.

The contribution to the energy associated with the new diagram is that of the old diagram multiplied by $(-1)^{n+m} = -1$. The new contribution is opposite in sign to the old one and the two topologically different diagrams cancel one another.

Corollary. For Hubbard's model of a narrow band, under the restrictive conditions prevailing in the above theorem, all Goldstone diagrams of odd order ($\neq 1$) in the perturbation vanish.

Proof. Since there is no interaction between like-spin particles in the Hubbard Hamiltonian, all odd-order diagrams must have at least one loop with an odd number ($\neq 1$) of particle lines. All these diagrams then cancel one another in view of the previous theorem. The only exceptions are the first-order diagrams of Fig. 1, which violate the said theorem.

APPENDIX D: VALIDITY OF GOLDSTONE EXPANSION

It was shown by Kohn and Luttinger[4] and by Luttinger and Ward[13] that the Goldstone expansion for the energy is generally incomplete for a nonspherical Fermi surface. We will endeavor to prove the Hubbard Hamiltonian in the tight-binding limit is an exception when the band is half-filled.

Kohn and Luttinger's arguments were based on a grand canonical formulation of the perturbation expansion. They took the zero-temperature limit after letting the volume go to infinity and found a difference between their expression for the energy and that from the Goldstone expansion:

$$E' = \lim_{T \to 0} \{ [\Omega_0(\mu) + \Omega_G(\mu) + \Omega_A(\mu) + N\mu] - [\Omega_0(\mu_0) + \Omega_G(\mu_0) + N\mu_0] \} . \tag{D1}$$

Here E' is the energy difference, μ is the chemical potential, μ_0 is the chemical potential in the zero-order approximation, N is the average number of electrons, Ω_0 is the thermodynamic potential of the unperturbed system, Ω_G is the contribution to the thermodynamic potential from the Goldstone diagrams, and Ω_A is the contribution to the thermodynamic potential from the anomalous diagrams. For a half-filled Hubbard band in the tight-binding limit, the chemical potential is

$$\mu = \tfrac{1}{2} I . \tag{D2}$$

This must be so from electron-hole symmetry. For this value of the chemical potential, the grand canonical Hamiltonian ($\mathcal{H} - \mu N$) is identical in the electron and hole representations thus assuring

half-occupancy of the band. If we choose the zero-order Hamiltonian to be the Hartree one, for which

$$\mu_0 = \tfrac{1}{2} I \,, \tag{D3}$$

while simultaneously removing the Hartree part of the interaction potential, we find no change in chemical potential as the interaction is turned on. On the other hand, there are no anomalous diagrams. All such diagrams would contain interaction lines between like-spin particles which is impossible in the Hubbard Hamiltonian. It is then easy to see that

$$E' = 0 \,, \tag{D4}$$

and under these conditions the Goldstone expansion for the energy is valid. But then the Goldstone energy is independent of any one-body potential that may be added to the unperturbed Hamiltonian and subtracted from the interaction part as long as the Fermi surface remains the same. Since this is the case for the Hartree potential in our analysis, we can safely conclude that the Goldstone expansion using the noninteracting Hamiltonian to zero order is also valid.

*Supported in part by the Office of Naval Research, Contract No. 78721 and by the Canadian National Research Council.

†Premanent address: Department of Physics, University of Sherbrooke, Sherbrooke, Quebec, Canada.

‡Permanent address: Department of Metallurgy, Mechanics and Materials Science and Department of Biophysics, Michigan State University, East Lansing, Mich. 48823.

[1]G. Kemeny and L. G. Caron, Rev. Mod. Phys. 40, 790 (1968).

[2]J. Hubbard, Proc. Roy. Soc. (London) A276, 238 (1961); A281, 401 (1964).

[3]B. D. Day, Rev. Mod. Phys. 39, 719 (1967).

[4]To first order in the perturbation one need not worry about possible breakdown of the Goldstone expansion due to nonsphericity of the Fermi surface. See W. Kohn and J. M. Luttinger, Phys. Rev. 118, 41 (1960).

[5]For the very special case of the half-filled Hubbard band in the tight-binding limit, it is shown in Appendix D that the Goldstone formalism is exact even though the Fermi surface is nonspherical.

[6]T. Matsubara and T. Yokota, in *Proceedings of the International Conference on Theoretical Physics, Kyoto and Tokyo*, 1953 (Science Council of Japan, Tokyo, 1954), p. 693.

[7]D. Adler, in *Solid State Physics*, edited by F. Seitz, D. Turnbull, and H. Ehrenreich (Academic, New York, 1968), Vol. 21.

[8]J. Des Cloizeaux, J. Phys. Radium 20, 606 (1959); 20, 751 (1959).

[9]D. R. Penn, Phys. Rev. 142, 350 (1966).

[10]N. F. Mott, Proc. Phys. Soc. (London) 62, 416 (1949); Can. J. Phys. 34, 1356 (1956); Nuovo Cimento Suppl. 7, 312 (1958); Rev. Mod. Phys. 40, 677 (1968).

[11]J. C. Slater, *Quantum Theory of Molecules and Solids*, (McGraw-Hill, New York, 1963), Vol. I.

[12]G. Kemeny and L. G. Caron, Phys. Rev. 159, 768 (1967).

[13]J. M. Luttinger and J. C. Ward, Phys. Rev. 118, 1417 (1960).

PHYSICAL REVIEW B VOLUME 3, NUMBER 9 1 MAY 1971

Supercurrent Density Distribution in Josephson Junctions

R. C. Dynes and T. A. Fulton
Bell Telephone Laboratories, Murray Hill, New Jersey 07974

(Received 19 November 1970)

The form of the modulation of the critical dc Josephson current I_c of a tunnel junction by an applied magnetic field B is shown to be uniquely related to the supercurrent density distribution within the junction integrated over the direction of B. This relation is used to quantitatively determine these "current-density profiles" from $I_c(B)$ measured for Sn-oxide-Sn junctions with barriers prepared by plasma-discharge oxidation and for the novel light-sensitive junctions described by Giaever, in which the tunneling barrier is formed by an evaporated film of CdS.

I. INTRODUCTION

In the field of tunneling between metals and semiconductors[1] the production of a uniform tunneling barrier has been a long-standing problem. Such techniques as thermal oxidation,[2] plasma-discharge oxidation,[3] anodization[4] or evaporation of thin insulating films[5] all have been employed. Usually at best only indirect evidence of the barrier perfection has been available.

A direct means of investigating this question is presented by the dc Josephson effect.[6,7] As Josephson has shown, a supercurrent can flow by the tunneling mechanism for junctions between two superconductors. The maximum supercurrent density that can flow at any point is proportional to the